Proceedings of the ASME 2017 36th International Conference on Ocean, Offshore and Arctic Engineering
OMAE2017
June 25-30, 2017, Trondheim, Norway

OMAE2017-61261

Time Varying Hydrodynamics Identification of a Flexible Riser under Multi-frequency Vortex-Induced Vibrations

Chang Liu
State Key Laboratory of Ocean Engineering,
Shanghai Jiao Tong University, Shanghai, China

Shixiao Fu*
State Key Laboratory of Ocean Engineering,
Shanghai Jiao Tong University, Shanghai, China
SINTEF Ocean, Trondheim, Norway

Mengmeng Zhang
State Key Laboratory of Ocean Engineering,
Shanghai Jiao Tong University, Shanghai, China

Haojie Ren
State Key Laboratory of Ocean Engineering,
Shanghai Jiao Tong University, Shanghai, China

ABSTRACT

In this paper, Forgetting Factor Recursive Least Squares (FF-LS) method is proposed to identify time-varying vortex-induced force coefficients of the flexible riser under multi-frequency VIV. FF-LS method introduces the forgetting factor, which gives more weight to the data closer to the present. This modification improves the method's sensitivity to the time-varying parameters, and enables it to identify the time-varying parameters under multi-frequency coupling. In this paper, the mass-spring-dashpot model is used to verify FF-LS method's ability to accurately identify time-varying parameters under multi-frequency coupling. Then, this methodology is used to identify the vortex-induced force coefficients of flexible riser at the basic frequency when vortex-induced vibration occurs. Identified coefficients are consistent with the result obtained from Least Squares method, which indicates that the proposed FF-LS method retrogrades to the Least Squares method when VIV response and the vortex-induced force contains only one single frequency. Finally, this methodology is used to identify the time-varying vortex-induced force coefficients of a flexible riser under VIV considering the coupling effect between the basic frequency and high frequency. The vortex-induced force reconstructed from identified time-varying coefficients is consistent with real vortex-induced force, which verifies the validity and applicability of this methodology in identifying time-varying vortex-induced force coefficients considering multi-frequency coupling effect. The results show that when the flexible riser is subjected to multi-frequency VIV, its vortex-induced force coefficients change periodically, the time-averaged values of these time-varying coefficients are different from the vortex-induced force coefficients at the basic frequency, which results from the coupling effect between the basic frequency and high frequency. Linear superposition of vortex-induced force coefficient at basic frequency and high frequency are different from time-varying coefficients considering coupling effect of multi-frequency and cannot reconstruct vortex-induced force correctly.

Key words: Vortex-induced vibration, Vortex-induced Force Coefficients, Forgetting factor Recursive Least Squares method

INTRODUCTION

When predicting Vortex-induced Vibration (VIV) of a flexible riser, the construction of the vortex-induced force directly determines the accuracy of VIV prediction results. The existing semi-empirical prediction model for VIV are based on the vortex-induced force coefficients database obtained from one degree of freedom forced oscillation test of rigid cylinder (pure CF or pure IL)[1, 2], which includes excitation coefficient and added-mass coefficient.

While in real case, VIV exists in both in-line (IL) direction and the crossflow (CF) direction, and VIV in these two directions are coupled to each other. This coupling of motion makes the VIV hydrodynamics in both directions influence each other. Jauvtis and Williamson [3] conducted a low mass-ratio two-dimensional free vibration experiment in order to reveal the characteristics of VIV responses considering coupling effect of CF direction and IL direction. It was found that the vortex shedding pattern is different from that of VIV in one-dimensional free vibration test. There are 2T vortex shedding modes in the wake vortex, that is, three vortices sheds from one side in

*Corresponding Author: Shixiao Fu, E-mail: shixiao.fu@sjtu.edu.cn, Shixiao.Fu@sintef.no

one period, which is the reason that the high frequency (three-order) component exists in lift force. Therefore, it is necessary to study vortex-induced force characteristics under the two-direction coupling. In order to obtain a database of VIV that can more accurately predict VIV response in CF direction of the riser. Dahl [4] carried out the two-dimensional forced oscillations of rigid cylinders. This experiment obtains the hydrodynamics coefficient database which can be used to predict the vortex-induced force of the riser, especially the third order high frequency vortex-induced force. However, the data contained in this database is relatively sparse, and the accuracy of vortex-induced vibration prediction based on this database has not been validated yet. In addition, how to use this method to study the hydrodynamic response of the flexible riser at high frequency should be further studied.

The rigid cylinder forced oscillation test can conveniently establish the hydrodynamic coefficient database for vortex-induced vibration prediction, but for the flexible riser, the coupling effect between CF and IL direction and the three-dimensional flow field effect make it different from the rigid cylinder [5, 6]. In flexible riser scaled model test, Vandiver [7, 8] found a high-order response at three times the basic frequency in the CF direction and four times the basic frequency in the IL direction, which indicates high-frequency vortex-induced force exists in a real flexible riser. This high-frequency force causes high-frequency VIV response. Wu and Lie et al.[9] obtained the vortex-induced force and its coefficient at the locking frequency in the CF direction of the riser using the beam finite element equation and the inverse analysis based on the optimal control theory. Song and Fu et al. [10] used the method of modal analysis combined with the Euler beam dynamic response equation to analyze hydrodynamic force. The strain information measured from flexible riser scaled model test is used to obtain the hydrodynamic characteristics at basic frequency. However, the hydrodynamic characteristics under the multi-frequency coupling are not analyzed in the above-mentioned papers.

For the vortex-induced force and VIV response at a single frequency, the vortex-induced force coefficient obtained by the least square method can be used to reconstruct the hydrodynamic force accurately. This method decomposes the hydrodynamic load into excitation force in phase with velocity and added-mass force in phase with the acceleration, which are normalized into excitation coefficient and added-mass coefficient, respectively. When high-order response exists in VIV response [8], or the use of buoyancy elements and strakes cause multiple basic frequencies to compete with each other [11-14], the vortex-induced force coefficients obtained by the least square method cannot accurately reconstruct the vortex-induced force, and cannot consider influence of multi-frequency coupling on hydrodynamic coefficient.

In order to overcome this shortcoming, this paper proposes a Forgetting Factor Least Square Method (FF-LS) for the identification of time-varying vortex-induced force coefficients of a flexible riser under multi-frequency VIV. The time-varying vortex-induced force coefficients are used to describe the coupling effects between multiple frequencies. This method introduces the forgetting factor, which gives a greater weight to the data closer to the present moment. This modification improves the sensitivity of the method to time-varying parameters, and makes it possible to identify the time-varying parameters under multi-frequency coupling. The time-varying vortex-induced force coefficients of the flexible riser is obtained through this method. The vortex-induced force coefficients under multi-frequency coupling and that at single frequency are compared and analyzed.

TIME-VARYING HYDRODYNAMICS AND ITS IDENTIFICATION

When flexible riser undergo vortex-induced vibration, the frequency where the power spectral density of VIV response in CF direction reaches maximum value is regarded as basic frequency (hereinafter all basic frequency are defined). Vibration in CF direction is usually composed of multi-frequency vibrations that are odd times of basic frequency $\omega, 3\omega, 5\omega\cdots$, while vibration in IL direction is usually composed of multi-frequency vibrations that are even times of basic frequency $2\omega, 4\omega, 6\omega\cdots$. The vibrations that are three times or more of basic frequency in CF direction and four times or more in IL direction are called high frequency response. [7] The response frequency is more complicated when considering buoyancy elements and strakes [14]. So this paper consider more general cases, where displacement response of the riser in CF and IL directions at node z are expressed as follows:

$$\begin{aligned} y(z,t) &= \sum y_i(z,t,\omega_i) \qquad i=1,2,3\cdots \\ x(z,t) &= x_0(z) + \sum x_i(z,t,\omega_i) \qquad i=1,2,3\cdots \end{aligned} \tag{1}$$

In above equation, $y_i(z,t,\omega_i)$ represents the displacement in CF direction at one single vibration frequency ω_i; $x_i(z,t,\omega_i)$ represents the displacement in IL direction at one single vibration frequency ω_i and $x_0(z)$ represents the average bending displacement.

In the following, a time-varying vortex-induced force coefficients model of flexible riser under multi-frequency VIV is established. The derivation of the vortex-induced force coefficients in IL direction is similar to that in CF

direction.

The displacement response in CF direction $y(z,t)$ of the riser at node z is written as a linear superposition of several single frequency responses:

$$\begin{aligned} y(z,t) &= \sum_i y_i(z,t,\omega_i) \\ &= \sum_i y_0(z,\omega_i)\sin(\omega_i t+\varphi_i) \quad i=1,2,3\cdots \end{aligned} \tag{2}$$

where ω_i is the i[th] circular frequency of the VIV response in CF direction; $y_0(z,\omega_i)$ is the displacement amplitude at the frequency ω_i; φ_i is the phase angle at the frequency ω_i. The VIV velocity and acceleration can be obtained by differentiating VIV displacement:

$$\begin{aligned} \dot{y}(z,t) &= \sum_i \dot{y}(z,t,\omega_i) \\ &= \sum_i \omega_i y_0(z,\omega_i)\cos(\omega_i t+\varphi_i) \\ \ddot{y}(z,t) &= \sum_i \ddot{y}(z,t,\omega_i) \\ &= -\sum_i \omega_i^2 y_0(z,\omega_i)\sin(\omega_i t+\varphi_i) \quad i=1,2,3\cdots \end{aligned} \tag{3}$$

In this case, the vortex-induced force in CF direction at node z can be expressed as:

$$\begin{aligned} f_{CF}(z,t) &= \sum_i f(z,t,\omega_i) \\ &= \sum_i f_0(z,\omega_i)\sin(\omega_i t+\varphi_i+\theta_i) \end{aligned} \tag{4}$$

where $f(z,t,\omega_i)$ is the vortex-induced force at frequency ω_i, $f_0(z,\omega_i)$ is the amplitude of vortex-induced force at frequency ω_i:

Expand this equation:

$$\begin{aligned} f_{CF}(z,t) &= \sum_i f_{CF}(z,t,\omega_i) \\ &= \sum_i f_0(z,\omega_i)\sin\theta_i\cos(\omega_i t+\varphi_i) \\ &\quad -[-\sum_i f_0(z,\omega_i)\cos\theta_i\sin(\omega_i t+\varphi_i)] \end{aligned} \tag{5}$$

where: $f_0(z,\omega_i)\sin\theta_i\cos(\omega_i t+\varphi_i)$ is the part of vortex-induced force in phase with velocity $\dot{y}(z,t,\omega_i)$ at corresponding frequency, namely excitation force:

$$\begin{aligned} &f_0(z,\omega_i)\sin\theta_i\cos(\omega_i t+\varphi_i) \\ &= \frac{\rho D l}{2\sqrt{2}\dot{y}_{RMS}(z,\omega_i)}U^2(z,t)CLe(z,\omega_i)\dot{y}(z,t,\omega_i) \end{aligned} \tag{6}$$

In above equation, l is the unit length; $CLe(z,\omega_i)$ is the excitation coefficient at the node z at frequency ω_i; ρ is the fluid density; $U(z,t)$ is the flow velocity at the node z at t moment; D is the hydrodynamic diameter of riser. $\dot{y}_{RMS}(z,\omega_i)$ is Root Mean Square (RMS) value of VIV velocity for node z at frequency ω_i:

$$\dot{y}_{RMS}(z,\omega_i)=\sqrt{\frac{1}{T}\int_0^T \dot{y}(z,t,\omega_i)^2 dt} \tag{7}$$

When the vortex-induced vibration of the riser is a single frequency harmonic response, $\sqrt{2}\dot{y}_{RMS}(z,\omega_i)$ is equal to the amplitude of the VIV velocity.

$$\sqrt{2}\dot{y}_{RMS}(z,\omega_i)=\dot{y}_0(z,\omega_i) \tag{8}$$

The term $-f_0(z,\omega_i)\cos\theta_i\sin(\omega_i t+\varphi_i)$ in equation (5) is the part of vortex-induced force in phase with acceleration $\ddot{y}(z,t)$, namely added-mass force, which can be expressed as:

$$\begin{aligned} &-f_0(z,\omega_i)\cos\theta_i\sin(\omega_i t+\varphi_i) \\ &= \frac{1}{4}\rho\pi D^2 l CLa(z,\omega_i)\ddot{y}(z,t,\omega_i) \end{aligned} \tag{9}$$

In this equation, $CLa(z,\omega_i)$ is the added-mass coefficient at the node z at frequency ω_i:

Substituting equation (6) and (9) into equation (5):

$$\begin{aligned} f_{CF}(z,t) &= \sum_i f_{CF}(z,t,\omega_i) \\ &= \sum_i \left[\begin{array}{c} \frac{\rho D l U^2(z,t)}{2\sqrt{2}\dot{y}_{RMS}(z,\omega_i)}CLe(z,\omega_i)\dot{y}(z,t,\omega_i) \\ -\frac{\rho\pi D^2 l}{4}CLa(z,\omega_i)\ddot{y}(z,t,\omega_i) \end{array}\right] \end{aligned} \tag{10}$$

In this equation, $CLe(z,\omega_i)$ and $CLa(z,\omega_i)$ are excitation coefficient and added-mass coefficient at node z at frequency ω_i in CF direction.

It can be seen from the above equation that when multi-frequency VIV occurs, excitation coefficients and added-mass coefficients at multi-frequency are needed to accurately reconstruct the vortex-induced force. In order to consider the coupling effect between the response and vortex-induced force at multiple frequencies, this paper solves time-varying hydrodynamic coefficients under multi-frequency coupling. Rewrite equation (10) as below:

$$\begin{aligned} f_{CF}(z,t) &= \frac{\rho D l U^2(z,t)}{2\sqrt{2}\dot{y}_{RMS}(z)}CLe(z,t)\dot{y}(z,t) \\ &\quad -\frac{\rho\pi D^2 l}{4}CLa(z,t)\ddot{y}(z,t) \end{aligned} \tag{11}$$

where

$$\begin{cases} \dot{y}(z,t)=\sum_i \dot{y}(z,t,\omega_i) & i=1,2,3,\cdots \\ \ddot{y}(z,t)=\sum_i \ddot{y}(z,t,\omega_i) & i=1,2,3,\cdots \\ f_{CF}(z,t)=\sum_i f_{CF}(z,t,\omega_i) & i=1,2,3,\cdots \\ \dot{y}_{RMS}(z)=RMS(\sum_i \dot{y}(z,t,\omega_i)) & i=1,2,3,\cdots \end{cases} \tag{12}$$

represents linear superposition of several velocity, acceleration, vortex-induced force and RMS value of

velocity superposition under multiple frequency.

$CLe(z,t), CLa(z,t)$ are time-varying excitation coefficient and added-mass coefficient, which replace the vortex-induced force coefficients at multiple frequencies $CLe_i(z,\omega_i), CLa_i(z,\omega_i)$ $i=1,2,3\cdots$ in equation (10). Time-varying vortex-induced force coefficients $CLe(z,t), CLa(z,t)$ take into account the vortex-induced force coefficients and the coupling effect among different frequencies.

When the above summing symbols contain only one single frequency response or force, the definition of hydrodynamic coefficients are consistent with the hydrodynamic coefficients defined by Gopalkrishnan [15]

Then the **Forgetting Factor Least Square method** (FF-LS) [16, 17] is introduced to identify the time-varying vortex-induced force coefficients in equation (11). This method introduces a forgetting factor, which gives a greater weight to the data close to the present moment. This modification improves the sensitivity of the Least Square method and makes it possible to identify the time-varying parameters under multi-frequency coupling accurately.

The solution model of Forgetting Factor Least Square is $\boldsymbol{f_L}=\boldsymbol{H_L}\boldsymbol{\theta}+\boldsymbol{n_L}$, where $\boldsymbol{f_L}$ is the output vector, $\boldsymbol{H_L}$ is the observable data matrix, $\boldsymbol{f}_L, \boldsymbol{H}_L$ are known, $\boldsymbol{\theta}(L)$ is unknown parameters at moment t_L, $\boldsymbol{n_L}$ is the uncorrelated random noise with zero mean value.

Assuming initial moment as t_1 and present moment as t_L, specific to the identification problem of vortex-induced force coefficient in this paper, $\boldsymbol{f_L}$ is the time history vortex-induced force at node z from initial moment t_1 to present moment t_L, $\boldsymbol{H_L}$ is the time history of velocity and acceleration at node z from initial moment t_1 to present moment t_L, $\boldsymbol{\theta}(L)$ is dimensional vortex-induced force coefficient at node z at moment t_L, namely:

$$\begin{aligned}
&\boldsymbol{f_L}=[f_{CF}(z,t_1), f_{CF}(z,t_2), f_{CF}(z,t_3),\cdots, f_{CF}(z,t_L)]^T\\
&\boldsymbol{H}_L=[\boldsymbol{h}(1),\boldsymbol{h}(2),\boldsymbol{h}(3),\cdots,\boldsymbol{h}(L)]^T\\
&\quad=\begin{bmatrix}\dot{y}(z,t_1),\dot{y}(z,t_2),\dot{y}(z,t_3),\cdots,\dot{y}(z,t_L)\\ \ddot{y}(z,t_1),\ddot{y}(z,t_2),\ddot{y}(z,t_3),\cdots,\ddot{y}(z,t_L)\end{bmatrix}^T\\
&\boldsymbol{\theta}(L)=\begin{bmatrix}\dfrac{\rho DU^2}{2\sqrt{2}\dot{y}_{RMS}(z)}CLe(z,t_L)\\ -\dfrac{\rho\pi D^2}{4}CLa(z,t_L)\end{bmatrix}\\
&L=1,2,3,\cdots
\end{aligned}\tag{13}$$

Time-varying vortex-induced force coefficient problem in equation (11) can be written as identifying the time history of a set of parameters

$\boldsymbol{\theta}(L)$ $L=1,2,3,\cdots$, which satisfy:

$$\boldsymbol{f}_L=\boldsymbol{H}_L\boldsymbol{\theta}(L)\quad L=1,2,3,\cdots \tag{14}$$

where $t_1,t_2,t_3,\cdots,t_L$ represents sampling time and totally L groups of data is sampled. Equation (14) shows all previous historical moments data before t_L are used to identify time-varying parameter $\boldsymbol{\theta}(L)$. In order to simplify the expression, the parameters $\boldsymbol{\theta}(L)$ at moment t_L are denoted as $\boldsymbol{\theta}$ in following description.

z represents the spatial position of the data, and the rows of the above three matrices represent the values at different sampling moment.

The data of output vector and observation matrix at different moment are multiplied by different data weights, and the data weight is bigger if the data is close to present moment t_L. Specifically, the data weight for the present moment is $\beta^0=1$, the data weight for the initial moment is β^{L-1} (β is a constant, which satisfy $0<\beta\le 1$). The output vector after multiplying data weight is:

$$\boldsymbol{f_L}^*=[\beta^{L-1}\boldsymbol{f}_L(1),\beta^{L-2}\boldsymbol{f}_L(2),\cdots\beta\boldsymbol{f}_L(L-1),\boldsymbol{f}_L(1)]^T \tag{15}$$

The same weighting process is applied to the data matrix:

$$\boldsymbol{H_L}^*=\begin{bmatrix}\beta^{L-1}\boldsymbol{h}^T(1)\\ \beta^{L-2}\boldsymbol{h}^T(2)\\ \\ \beta\boldsymbol{h}^T(L-1)\\ \boldsymbol{h}^T(L)\end{bmatrix} \tag{16}$$

So the solution model is rewritten as follows:

$$\boldsymbol{f_L}^*=\boldsymbol{H_L}^*\boldsymbol{\theta}+\boldsymbol{n_L}^* \tag{17}$$

According to the basic principle of Least Square method [18], the parameters to be identified need to minimize the sum squared errors between $\boldsymbol{H_L}^*\boldsymbol{\theta}(L)$ and $\boldsymbol{f_L}^*$, namely:

$$\min J(\boldsymbol{\theta})=(\boldsymbol{f_L}^*-\boldsymbol{H_L}^*\boldsymbol{\theta})^T(\boldsymbol{f_L}^*-\boldsymbol{H_L}^*\boldsymbol{\theta}) \tag{18}$$

Assuming $\hat{\boldsymbol{\theta}}(L)_{WLS}$ satisfy $J(\boldsymbol{\theta}(L))\big|_{\theta(L)_{WLS}}=\min$, there is

$$\frac{\partial J(\boldsymbol{\theta})}{\partial\boldsymbol{\theta}}\bigg|_{\hat{\theta}_{WLS}}=\frac{\partial}{\partial\boldsymbol{\theta}}(\boldsymbol{f_L}^*-\boldsymbol{H_L}^*\boldsymbol{\theta})^T(\boldsymbol{f_L}^*-\boldsymbol{H_L}^*\boldsymbol{\theta})\bigg|_{\hat{\theta}_{WLS}}=\boldsymbol{\theta}^T \tag{19}$$

Expand above equation and use the following two vector differential formula:

$$\begin{cases}\dfrac{\partial}{\partial\boldsymbol{x}}(\boldsymbol{\alpha}^T\boldsymbol{x})=\boldsymbol{\alpha}^T\\ \dfrac{\partial}{\partial\boldsymbol{x}}(\boldsymbol{x}^T\boldsymbol{A}\boldsymbol{x})=2\boldsymbol{x}^T\boldsymbol{A}\end{cases} \tag{20}$$

Equation (19) becomes:

$$(\boldsymbol{H_L}^{*T}\boldsymbol{H_L}^*)\hat{\boldsymbol{\theta}}_{WLS}=\boldsymbol{H_L}^{*T}\boldsymbol{f_L}^* \tag{21}$$

The above equation is called regular equation, and

when $\boldsymbol{H}_L^{*T}\boldsymbol{H}_L^{*}$ is a regular matrix, it gets:

$$\hat{\boldsymbol{\theta}}_{WLS}=(\boldsymbol{H}_L^{*T}\boldsymbol{H}_L^{*})^{-1}\boldsymbol{H}_L^{*T}\boldsymbol{f}_L^{*} \tag{22}$$

Substituting equation (15) (16) into equation (22):

$$\begin{aligned}\hat{\boldsymbol{\theta}}(L)&=\left[\sum_{i=1}^{L}\beta^{2(L-i)}\boldsymbol{h}(i)\boldsymbol{h}^{\boldsymbol{T}}(i)\right]^{-1}\left[\sum_{i=1}^{L}\beta^{2(L-i)}\boldsymbol{h}(i)z(i)\right]\\&=\left[\sum_{i=1}^{L}\mu^{(L-i)}\boldsymbol{h}(i)\boldsymbol{h}^{\boldsymbol{T}}(i)\right]^{-1}\left[\sum_{i=1}^{L}\mu^{(L-i)}\boldsymbol{h}(i)z(i)\right]\\&=(\boldsymbol{H}_L^{\ T}\boldsymbol{\Lambda}_L\boldsymbol{H}_L)^{-1}\boldsymbol{H}_L^{\ T}\boldsymbol{\Lambda}_L\boldsymbol{f}_L\end{aligned} \tag{23}$$

Where $\mu=\beta^2$, $0<\mu\le 1$, μ is called **Forgetting Factor**, $\boldsymbol{\Lambda}_L$ is weighted matrix, whose diagonal elements are $\Lambda(L)=1$, $\Lambda(k-1)=\mu\Lambda(k)$, non-diagonal elements is 0. The essence of this method is to give different weights to the data, the farther away from the present moment of data, the smaller the weight, as shown below:

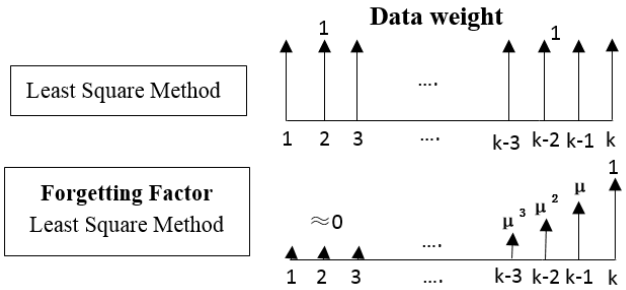

Figure 1 Schematic of data weight for forgetting factor least square method

VERIFICATION OF IDENTIFICATION METHOD

In order to verify that Forgetting Factor Least Square method proposed in this paper can accurately identify the time-varying vortex-induced force coefficients under multi-frequency coupling, this part uses the mass-spring-dashpot model to verify this method. The following problem is constructed:

The motion signal $y(t),\dot{y}(t),\ddot{y}(t)$ and the real force signal $F_{real}(t)$ are known, which satisfies the equation:

$$M*\ddot{y}(t)+C*\dot{y}(t)+K*y(t)=F_{real}(t) \tag{24}$$

where M,C,K are mass, damping of the dashpot and stiffness of spring, respectively, and they are constant.

According to the vortex-induced force decomposition method of the flexible riser, the real force signal can be decomposed into excitation force $F_v(t)=CLe(t)*\dot{y}(t)$ related to velocity and added-mass force $F_a(t)=CLa(t)*\ddot{y}(t)$ related to acceleration, namely:

$$F_{recon}(t)=CLe(t)\dot{y}(t)+CLa(t)*\ddot{y}(t) \tag{25}$$

$CLe(t)$ and $CLa(t)$ are called excitation coefficient and added-mass coefficient of mass-spring-dashpot system. Similar to the identification of vortex-induced force coefficient of flexible riser, the sum of squared errors between force signal reconstructed from the identified coefficients $F_{recon}(t)=CLe(t)*\dot{y}(t)+CLa(t)*\ddot{y}(t)$ and real force signal should be minimized:

$$\min[F_{real}(t)-F_{recon}(t)]^2 \tag{26}$$

The verification idea is as follows: Firstly, we know the response and force signals of single frequency and coefficients are identified by Least Square method and Forgetting Factor Least Square method proposed in this paper to verify they are consistent with the theoretical results. Secondly, we know the motion signal and force signal of multi-frequency (two frequencies) and coefficients are identified by LS method and Forgetting Factor Least Square method, respectively. Comparing force signal reconstructed from the identified coefficients with real force signal, the correctness and superiority of Forgetting Factor Least Square method proposed in this paper are verified.

Single Frequency Response

We set $M=10$, $C=40$, $K=1500$ and simulate motion of 20s taking an observation data each 0.01s.

Motion signals are set as:

$$\begin{cases}y(t)=A\sin(2\pi ft+\varphi)\\ \dot{y}(t)=2\pi fA\cos(2\pi ft+\varphi)\\ \ddot{y}(t)=-(2\pi f)^2A\sin(2\pi ft+\varphi)\end{cases} \tag{27}$$

where vibration amplitude is taken as $A=0.01$,the vibration frequency is taken $f=1Hz$, the initial phase angle is taken as $\varphi=0°$

Substituting above motion signal into dynamics equation of mass-spring-dashpot model (24):

$$\begin{aligned}F_{real}(t)&=M\ddot{y}(t)+C\dot{y}(t)+Ky(t)\\&=[-MA(2\pi f)^2+KA]\sin(2\pi ft+\varphi)\\&\quad+2\pi fCA\cos(2\pi ft+\varphi)\end{aligned} \tag{28}$$

Minimizing squared errors between reconstructed force and real force:

$$\begin{aligned}&\min[F_{real}(t)-F_{fit}(t)]^2\\&=[F_{real}(t)-CLe(t)\dot{y}(t)-CLa(t)\ddot{y}(t)]^2\end{aligned} \tag{29}$$

Substituting motion and force signal in equation (27) (28) into (29):

$$\begin{aligned}&\min[F_{real}(t)-F_{fit}(t)]^2\\&=\{-MA(2\pi f)^2+KA]\sin(2\pi ft+\varphi)\\&\quad+2\pi fCA\cos(2\pi ft+\varphi)\\&\quad-CLe(t)*2\pi fA\cos(2\pi ft+\varphi)\\&\quad-CLa(t)*[-(2\pi f)^2A\sin(2\pi ft+\varphi)]\}^2\end{aligned} \tag{30}$$

Because the trigonometric function set $\{\cos n\omega_1 t, \sin n\omega_1 t\}(n=0,1,2,\cdots,\infty)$ constitute a complete orthogonal function set in interval (t_0, t_0+T_1) where $T_1=\frac{2\pi}{\omega_1}$, namely:

$$\begin{aligned}
&\int_{t_0}^{t_0+T} \cos m\omega_1 t \cos n\omega_2 t dt = 0 (m \neq n) \\
&\int_{t_0}^{t_0+T} \sin m\omega_1 t \sin n\omega_2 t dt = 0 (m \neq n) \\
&\int_{t_0}^{t_0+T} \cos m\omega_1 t \sin n\omega_2 t dt = 0
\end{aligned} \tag{31}$$

So the theoretical solution of equation (30) is obtained:

$$\begin{cases} CLe(t) = C = 40 \\ CLa(t) = \dfrac{-MA(2\pi f)^2 + KA}{-A(2\pi f)^2} = -27.995 \end{cases} \tag{32}$$

For the above motion and force signal at single-frequency, the Least Square and Forgetting Factor Least Square method are performed to identify the excitation coefficient and the added-mass coefficient, respectively. Their comparison with theoretical solution is shown in table below:

Table 1 Excitation coefficient and added-mass coefficient at single frequency (Theoretical results, results obtained by Least Square method and results obtained by Forgetting Factor Least Square method)

Parameter	Theoretical Result	LS Result	FF-LS Result
$CLe(t)$	40	39.66	39.75
$CLa(t)$	-27.995	-27.69	-27.97

The results are consistent with the theoretical results, and the results are consistent with the results obtained from Least Square method. These results show that FF-LS retrogrades to LS method when dealing with single frequency signals. The correctness of this method is further illustrated by reconstructing force signal from identified coefficients, which matches the real force signal. (Figure 2)

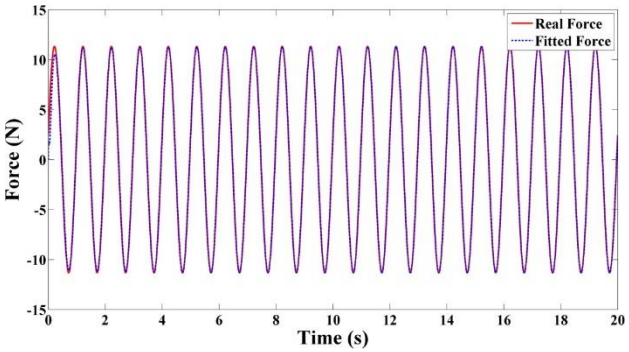

Figure 2 Comparison between real force and force reconstructed from identified coefficients

Multiple Frequency Response

We set $M=10$, $C=40$, $K=1500$ and simulate motion of 20s taking an observation data each 0.01s.

Motion signals are set as:

$$\begin{cases} y(t) = A_1 \sin(2\pi f_1 t + \varphi_1) + A_2 \sin(2\pi f_2 t + \varphi_2) \\ \dot{y}(t) = 2\pi f_1 A_1 \cos(2\pi f_1 t + \varphi_1) \\ \qquad + 2\pi f_2 A_2 \cos(2\pi f_2 t + \varphi_2) \\ \ddot{y}(t) = -(2\pi f_1)^2 A_1 \sin(2\pi f_1 t + \varphi_1) \\ \qquad - (2\pi f_2)^2 A_2 \sin(2\pi f_2 t + \varphi_2) \end{cases} \tag{33}$$

where vibration amplitudes $A_1=0.01$, $A_2=0.005$, vibration frequencies $f_1=1Hz$, $f_2=3f_1=3Hz$, the corresponding circle frequency is $\omega_1=2\pi f_1$, $\omega_2=2\pi f_2$, initial phase angle is $\varphi_1=\varphi_2=0$

Figure 3 and Figure 4 is time history and power spectral density (PSD) of motion signal under multi-frequency superposition. It can be seen that the PSD of high-frequency components is equal to or higher than PSD of low-frequency components in velocity and acceleration, even though the displacement amplitude of high-frequency motion is small.

Equation (24) is used to construct the real force corresponding to motion signal. For multi-frequency motion response, the coefficients identification problem in equation (34) do not have theoretical solution:

$$\begin{aligned}
&\min[F_{real}(t) - F_{fit}(t)]^2 \\
&= [F_{real}(t) - CLe(t)\dot{y}(t) - CLa(t)\ddot{y}(t)]^2
\end{aligned} \tag{34}$$

The results obtained from Least Square method is $CLe(t)=39.55,\ CLa(t)=4.187$, but the force signal reconstructed from these two coefficients are different from real force (Figure 5). When considering coupling effect between multiple frequencies, using steady excitation coefficient and added-mass coefficient is not sufficient to accurately reconstruct force signal.

The time-varying excitation coefficient and added-mass coefficient of the mass-spring-dashpot model are

obtained by Forgetting Factor Least Square method. The force signal reconstructed from time-varying coefficients matches well with real force (Figure 5). In this case, excitation coefficient and added-mass coefficient will change periodically over time, which is caused by coupling effect between multiple frequencies. The results show that the Forgetting Factor Least Square method proposed in this paper can effectively identify time-varying parameters when consider multi-frequency coupling effect.

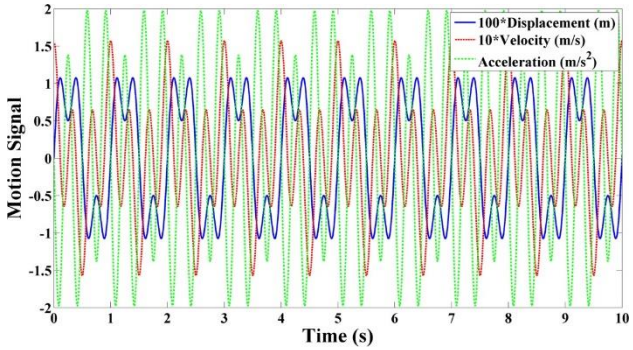

Figure 3 Time history of motion superposition under ω_1 and ω_2 (displacement, velocity and acceleration)

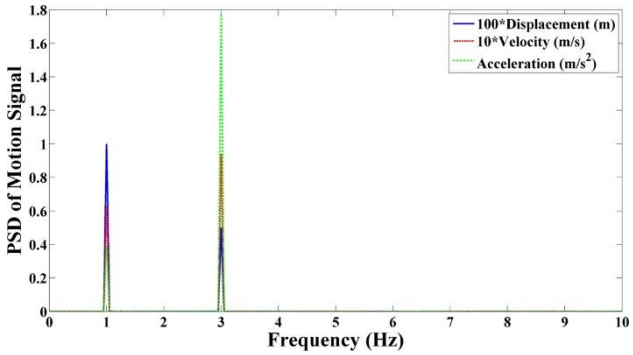

Figure 4 Power spectral density of motion superposition under ω_1 and ω_2 (displacement, velocity and acceleration)

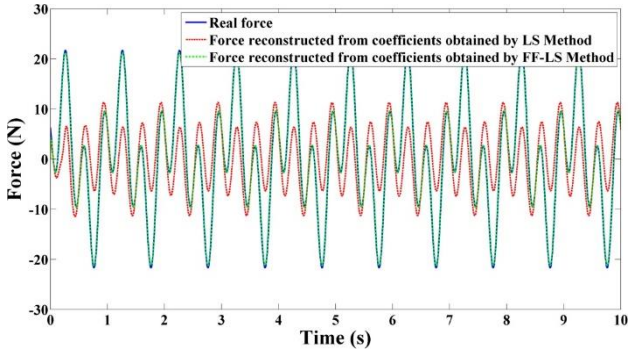

Figure 5 Comparison among real force, force reconstructed from coefficients identified by LS method and that identified by FF-LS method

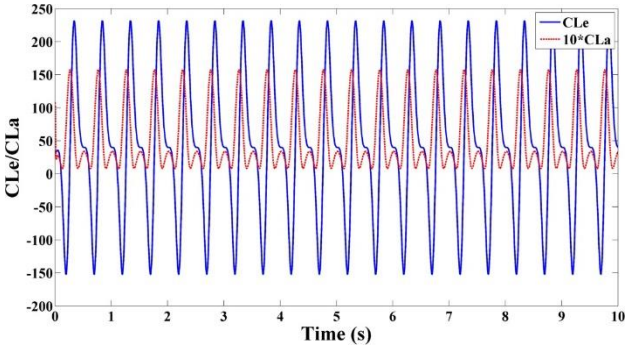

Figure 6 Time history of excitation coefficient and added-mass coefficient in mass-spring-dashpot system

TIME-VARYING HYDRODYNAMICS OF FLEXIBLE RISER UNDER MULTI-FREQUENCY VIV

Model Test

The experiments were performed in the towing tank, where a flexible riser was horizontally towed with constant speed to simulate a uniform flow. The two end of the riser were connected to the towing carriage with universal joints, and maintain a constant pre-tension. The experimental setup is shown in Figure 7

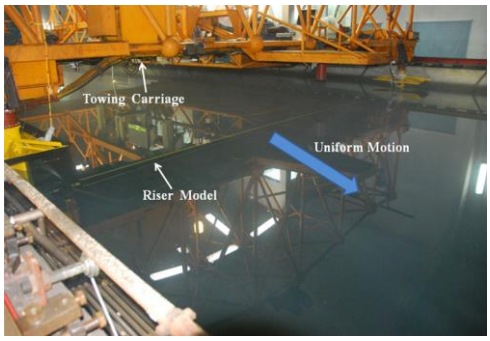

Figure 7 Testing setup for a flexible riser in a uniform flow

The hydrodynamic diameter of scaled riser was 31 mm with an effective length of 7.9m. The slenderness ratio of this riser was 263, and other structural parameters are shown in Table 2

Table 2 Parameters of the riser model

Parameter	Value	Parameter	Value
Hydrodynamic diameter（m）	0.031	Structural damping ratio（%）	0.3
Diameter（m）	0.03	Axial stiffness（N）	1.45E7
Inner diameter（m）	0.027	Bending stiffness（N.m^2）	1.48E3
Mass per unit length（Kg/m）	1.768	Pretension（N）	2943

Structural damping ratio in above table is structural damping ratio in air, which was obtained from free-decay

test in air.

In the experiment, FBG strain gauges were used to measure the strain response of the riser model. The FBG strain sensors are arranged in the CF1, CF2, IL1, and IL2 directions of the riser model, and are used to measure the strain in the four directions of the model, namely εCF1, εCF2, εIL1 and εIL2, which is shown in Figure 8. Totally 88 Fiber Bragg grating (FBG) strain sensors were instrumented on the surface of the riser model in both CF and IL planes. The strain sensor is embedded into the glass fiber with an outer diameter of 125–140 mm, and the fiber was then glued onto the surface of the riser model. Additionally, a thin sleeve plastic tube was finally covered outside the riser model to ensure the smooth surface of the riser. Therefore, the FBG strain sensors would not affect the flow around the vibrating riser and the vibration characteristics of the flexible riser. In addition, in the experiment, the strain information of all measuring points in the four directions on the riser model is collected at the same time, so there is no phase delay between the measured information at different measuring points.

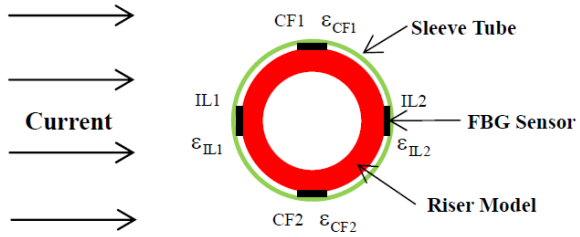

Figure 8 Arrangement of strain gauges on the surface of the riser model

In this paper, the representative experimental conditions are selected: the vortex-induced vibration response of the CF direction under 2.8m/s uniform flow is analyzed to illustrate the feasibility and correctness of this method. The corresponding Reynolds number is $6.4*10^4$.

VIV Response and Vortex-induced Force

A submerged flexible riser with a tensional force in a uniform current is illustrated in Figure 9(a). [10] The central axis of the riser lies on the Z-axis. The direction of the flow is parallel to X–Z plane and orthogonal to the riser. The time-invariant mean drag force acts on the riser in IL plane, which causes the riser a mean deflection in the flow direction. This deflection will be referred to as the initial bending, and the corresponding position of the riser will be referred to as the equilibrium position, as illustrated by Figure 9(b). As the fluid flows over the riser, vortices form and are shed periodically. This vortex shedding generates periodic vortex-induced forces in CF and IL planes with mean values of zero, and causes the riser to vibrate in the two planes, which is called vortex-induced vibration (VIV), as illustrated by Figure 9(b) and (c). Correspondingly, the hydrodynamic forces on a flexible riser shall also include three parts: vortex-induced forces in CF and IL directions, and mean drag force in the IL direction.

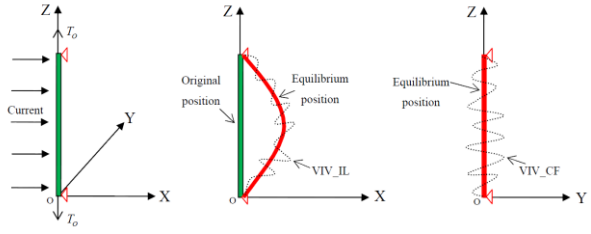

Figure 9 Response of a submerged flexible riser with a tensional force under uniform flow

According to FEM, the governing equation of spatial beam can be expressed as,

$$M\delta'' + C\delta' + K\delta = F \qquad (35)$$

where M, C and K are global mass matrix, damping matrix and stiffness matrix of the riser, respectively; δ ,δ' and δ'' are the displacement matrix, velocity matrix and acceleration matrix, respectively; F is the hydrodynamic force matrix. For a riser with N nodes and 6 degrees of freedom at each node, the dimensions of M、C、K are $6N \times 6N$ and the dimensions of δ and F are $6N \times 1$.

The stiffness matrix K^e of riser with a tensional force including two parts:

$$K^e = K_a^e + K_b^e \qquad (36)$$

Where K_a^e is the prestressed stiffness matrix caused by axial tension of the riser, and the K_b^e is the small displacement linear stiffness matrix caused by riser bending stiffness. The damping matrix C of riser can be solved by Rayleigh damping model:

$$C = \alpha * M + \beta * K \qquad (37)$$

Where α and β are Rayleigh damping coefficient which can be derived by natural frequency and structural damping ratio of riser.

The displacement matrix δ of riser can be expressed as

$$\delta = [\delta_1, \delta_2, \ldots, \delta_N]^T \ (i = 1 \sim N) \qquad (38)$$

where N is the node number, δ_i is the displacement vector of riser at node i

$$\delta_i = \begin{bmatrix} z_i & x_i & y_i & \theta_{zi} & \theta_{yi} & \theta_{xi} \end{bmatrix}^T \qquad (39)$$

where z_i is the axial displacement at node i; x_i and y_i are the bending displacements in IL and CF directions at node i, respectively; θ_{zi} is the torsion angle of riser around the axis, namely Z-axis; θ_{yi} and θ_{xi} are the angular

displacement around *Y*-axis and *X*-axis, which are induced by the vibration in IL and CF directions, respectively. In the following hydrodynamic forces analysis, the impact of axial elongation and torsion is neglected, i.e. $z_i = 0$ and $\theta_{zi} = 0$.

The axial tensile displacement of the riser can be calculated from the tensile strain of the riser surface; the bending displacement in the IL and CF directions can be obtained from the bending strain of the standpipe surface using modal analysis [19]. The bending strain and bending displacement of riser CF and IL are shown in Appendix A.

With displacement matrix δ, the velocity matrix δ' and acceleration matrix δ'' can be obtained by using the central-difference method to calculate the first- and the second-order partial derivatives of δ with respect to time.

After obtaining the structural response matrixes $\delta, \delta', \delta''$, and mass matrix M, stiffness matrix K and damping matrix C, the hydrodynamic force *F* on the right side of Equation (35) can be obtained by the inverse analysis.

Figure 10 is the time-space distribution of VIV strain, and Figure 11 is Power Spectral Density (PSD) distribution of VIV strain. The results showed that VIV strain in CF direction contains multiple frequency components. The frequency that has the maximum power spectral density of the VIV strain is the basic frequency $\omega_1 = 2\pi * f_1 = 2\pi * 16.8\ rad/s$. At the same time, the high-frequency (three times of basic frequency) response also appear and it is denoted as $\omega_2 = 2\pi * f_2 = 2\pi * 50.4\ rad/s$. Some other frequency components, such as half basic frequency and twice basic frequency also appear. Because this paper focuses on verifying the method that take into account the coupling effect of multi-frequency, the latter two components are not considered in this paper.

The VIV displacement reconstructed from modal analysis also contain multiple frequency components. (Figure 12). Vortex-induced force of riser is reconstructed from VIV displacement by inverse finite element theory. This force is denoted as real force below. Figure 13 to Figure 14 are time-space distribution and PSD distribution of vortex-induced force, respectively. The results show that high-frequency vortex-induced force at three times of basic frequency 3ω also appears. Dahl [4] also found vortex-induced force at three times of basic frequency in two-dimensional free vibration test of rigid cylinder and 2T vortex shedding pattern of two dimensional motion in high Re number contribute to this high-frequency force.

The PSD distribution of vortex-induced force (Figure 14) also indicate that high-frequency components cannot be neglected.

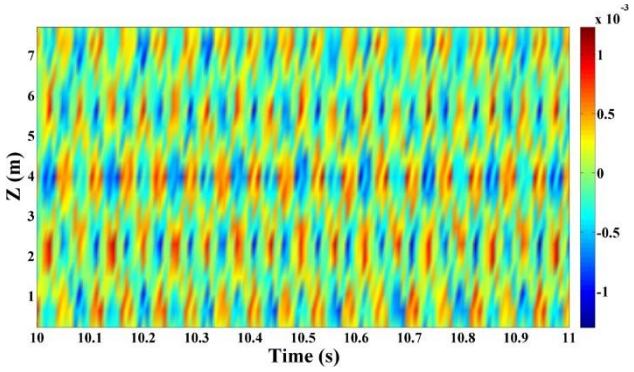

Figure 10 Time-space distribution of VIV strain

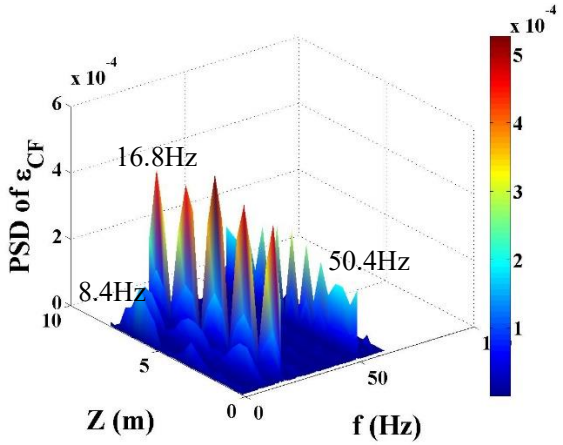

Figure 11 PSD distribution of VIV strain

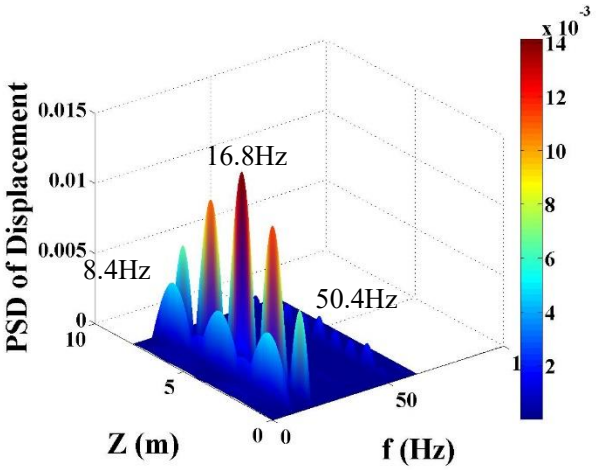

Figure 12 PSD distribution of VIV displacement

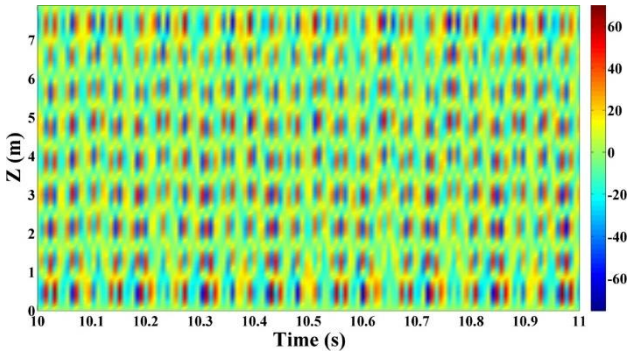

Figure 13 Time-space distribution of vortex-induced force

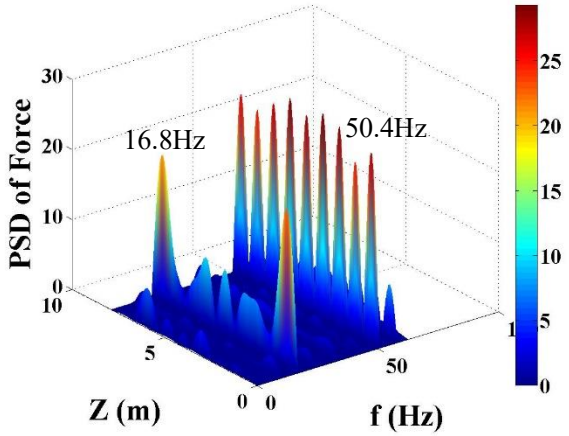

Figure 14 PSD distribution of vortex-induced force

Single Frequency

This section decomposes the vortex-induced force, VIV velocity and VIV acceleration into components at basic frequency $\omega_1 = 2\pi * 16.8\ rad/s$ and high frequency $\omega_2 = 2\pi * 50.4\ rad/s$ through bandpass filtering. Filter bandwidth is $16Hz \sim 17.5Hz$ and $50.1Hz \sim 50.7Hz$

Figure 15 to Figure 16 are time-space distribution of vortex-induced force at basic frequency ω_1 and axial distribution of RMS value of vortex-induced force (comparing the force before filter and force at basic frequency). Time history of vortex-induced force and axial distribution of RMS value of vortex-induced force at basic frequency have a large difference from those before filter. VIV response: displacement, velocity and acceleration are processed using the same method and similar phenomenon is observed.

Afterwards, vortex-induced force coefficients are identified through FF-LS method and LS method, respectively according to equation (11). Identified vortex-induced force coefficient at basic frequency do not change over time and the coefficients identified by FF-LS is consistent with that identified by Least Square method (Figure 17 and Figure 18). Figure 19 shows force reconstructed from identified coefficients by FF-LS are consistent with real force at basic frequency. These results indicate the correctness of Forgetting Factor Least Square method proposed in this paper and this method retrograde into Least Square method when processing single frequency VIV response.

The vortex-induced force and VIV response at high-frequency $\omega_2 = 2\pi * 50.4\ rad/s$ are obtained by bandpass filter. Figure 20 to Figure 21 are time-space distribution and axial distribution of RMS value of vortex-induced force at high-frequency ω_2. High frequency components contribute a lot in vortex-induced force, but it is still different from vortex-induced force before filtering. The reason is that in this case, the contribution of basic frequency is not taken into account. Similar conclusion can be obtained for VIV displacement, velocity and acceleration at high frequency.

Figure 22 to Figure 23 shows that the coefficients identified by FF-LS is consistent with that identified by Least Square method. Figure 24 shows force reconstructed from identified coefficients by FF-LS are consistent with real force at high frequency. These results further verify the correctness of FF-LS method proposed in this paper, which indicate it is also suitable to process vortex-induced force coefficient at high frequency.

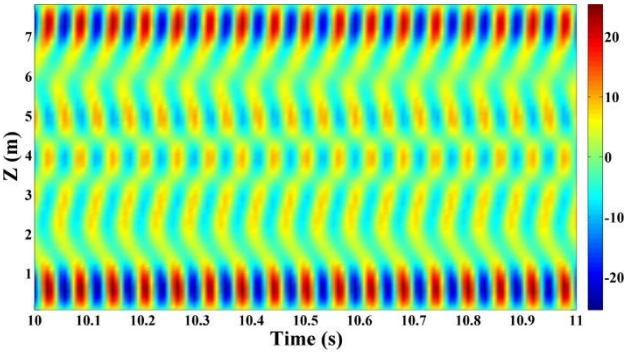

Figure 15 Time-space distribution of vortex-induced force at basic frequency ω_1

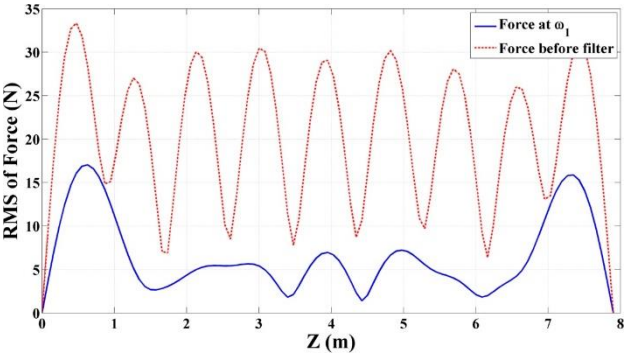

Figure 16 Axial distribution of RMS value of vortex-induced force (red dotted line: before filter, blue solid line: basic frequency ω_1)

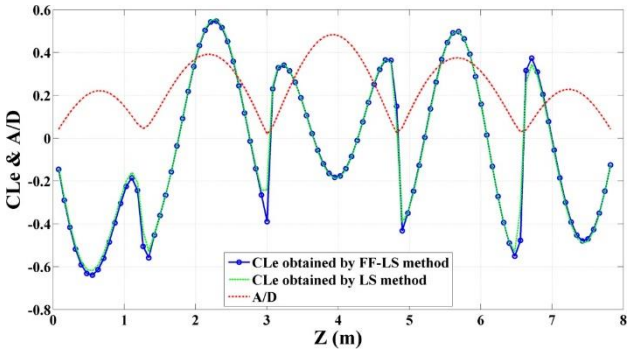

Figure 17 Axial distribution of excitation coefficient at basic frequency ω_1 and RMS value of dimensionless displacement (blue solid line: Forgetting Factor Least Square method, green dotted line: Least Square method)

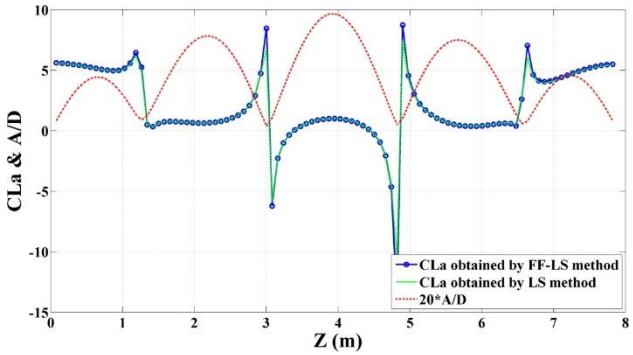

Figure 18 Axial distribution of added-mass coefficient at basic frequency ω_1 and RMS value of dimensionless displacement (blue solid line: Forgetting Factor Least Square method, green dotted line: Least Square method)

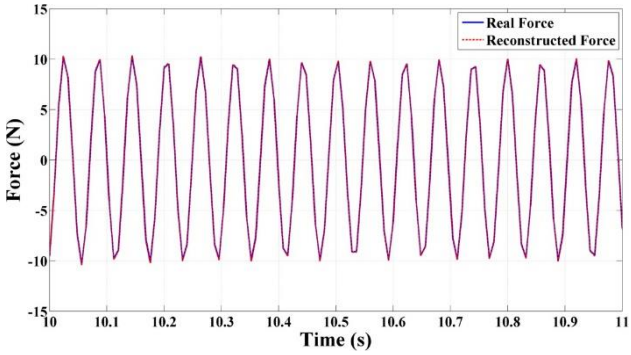

Figure 19 Comparison between real vortex-induced force and force reconstructed from identified vortex-induced force coefficients (basic frequency ω_1)

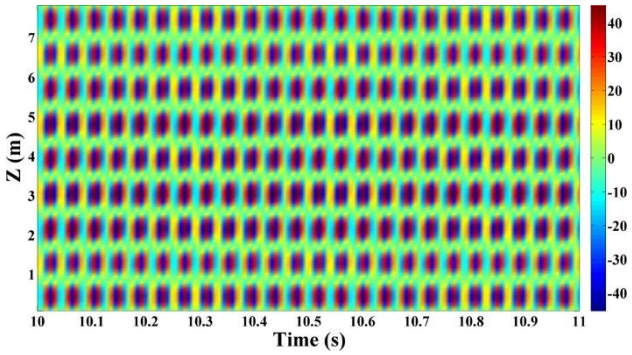

Figure 20 Time-space distribution of vortex-induced force at high frequency ω_2

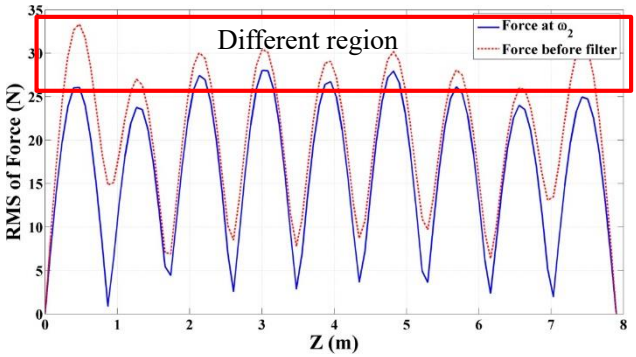

Figure 21 Axial distribution of RMS value of vortex-induced force (red dotted line: before filter, blue solid line: high frequency ω_2)

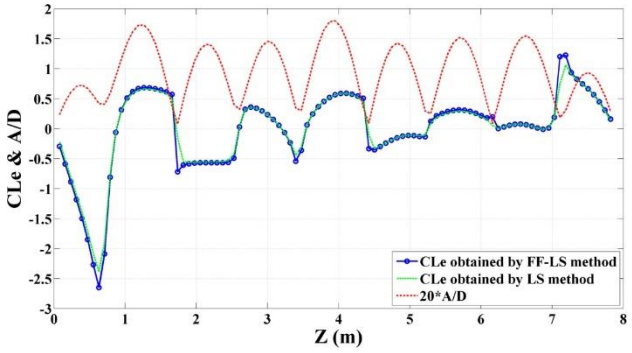

Figure 22 Axial distribution of excitation coefficient at high frequency ω_2 and dimensionless displacement (blue solid line: Forgetting Factor Least Square, green dotted line: Least Square)

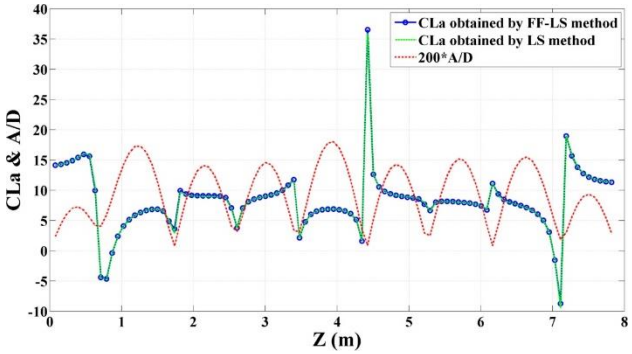

Figure 23 Axial distribution of added-mass coefficient at

high frequency ω_2 and dimensionless displacement (blue solid line: Forgetting Factor Least Square, green dotted line: Least Square)

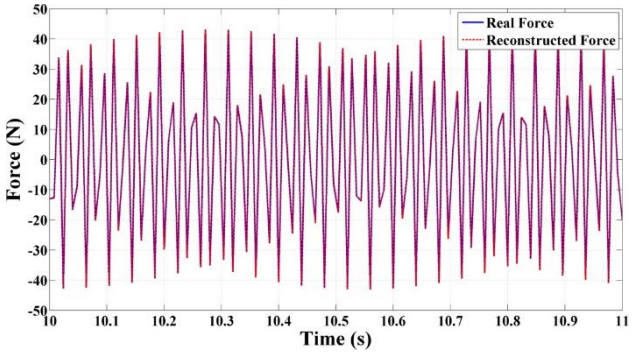

Figure 24 Comparison between real vortex-induced force and force reconstructed from identified coefficients (high frequency ω_2)

Multiple Frequency Coupling

In order to verify that FF-LS method can be used to solve the time-varying vortex-induced force coefficients under multi-frequency coupling, this section calculate the linear superposition of VIV response at basic frequency and high frequency. Vortex-induced force is also processed in the same way, namely:

$$\begin{cases} y_{multi}(z,t) = y(z,t,\omega_1) + y(z,t,\omega_2) \\ \dot{y}_{multi}(z,t) = \dot{y}(z,t,\omega_1) + \dot{y}(z,t,\omega_2) \\ \ddot{y}_{multi}(z,t) = \ddot{y}(z,t,\omega_1) + \ddot{y}(z,t,\omega_2) \\ F_{multi}(z,t) = F(z,t,\omega_1) + F(z,t,\omega_2) \end{cases} \tag{40}$$

Figure 25 is time-space distribution of vortex-induced force superposition under basic frequency ω_1 and high frequency ω_2. Comparing it with time-space distribution of vortex-induced force before filter in Figure 13, it is found that force superposition under basic frequency ω_1 and high frequency ω_2 can represent characteristics of real vortex-induced force. Figure 26 is axial distribution comparison of RMS value between force before filter and force superposition under basic frequency ω_1 and high frequency ω_2. When only considering basic frequency ω_1 and high frequency ω_2, the RMS value of force superposition is smaller than that of force before filter. Contribution of other frequency components (e.g. twice basic frequency components) results in this difference.

Substituting equation (40) into time-varying vortex-induced force model in equation (11), the vortex-induced force coefficient $CLe(z,t), CLa(z,t)$ should satisfy:

$$F_{multi}(z,t) = \frac{\rho D l U^2(z,t)}{2\sqrt{2}v_{RMS}(z)} CLe(z,t)\dot{y}_{multi}(z,t) - \frac{\rho\pi D^2 l}{4} CLa(z,t)\ddot{y}_{multi}(z,t) \tag{41}$$

Then time-varying vortex-induced force coefficients are identified by Forgetting Factor Least Square method.

Figure 27 and Figure 28 are time-space distribution of excitation coefficient and added-mass coefficient. These figures show that excitation coefficient and added-mass coefficient will change periodically over time, and it contain multiple frequency components.

Figure 29 and Figure 30 are axial distribution of excitation coefficient and added-mass coefficient at different moment. For time-varying effects result from coupling effect of multi-frequency, the axial distribution of vortex-induced force coefficients vary greatly at different moments.

Figure 31 and Figure 32 are axial distribution of excitation coefficient and added-mass coefficient (red hollow round: Time-average of excitation coefficient under coupling between basic frequency ω_1 and high frequency ω_2, blue plus: basic frequency ω_1, black diamond: Superposition of excitation coefficient at basic frequency ω_1 and high frequency ω_2)

Comparing these results, it is concluded:

1) The vortex-induced force coefficient at high frequency is much larger than that at basic frequency.

2) Time-average value of vortex-induced force coefficient under multi-frequency coupling are different from vortex-induced force coefficient at basic frequency, which results from coupling effect from high frequency.

In order to verify the correctness of identified time-varying vortex-induced force coefficients $CLe(z,t)$, $CLa(z,t)$, using these coefficients to reconstruct vortex-induced force as below equation:

$$F_{Recon}(z,t) = \frac{\rho D l U^2(z,t)}{2\sqrt{2}v_{RMS}(z)} CLe(z,t)\dot{y}_{multi}(z,t) - \frac{\rho\pi D^2 l}{4} CLa(z,t)\ddot{y}_{multi}(z,t) \tag{42}$$

where the definition of $\dot{y}_{multi}(z,t)$, $\ddot{y}_{multi}(z,t)$ can be seen in equation (40)。

Time-space distribution of reconstructed force is shown in Figure 33, which is consistent with real force $F_{multi}(z,t)$ in this case (Figure 25). Figure 34 is time history of reconstructed force and real force at the midpoint of riser. They match well with each other. These results indicate time-varying vortex-induced force coefficients identified by FF-LS method can reproduce distribution characteristics of vortex-induced force.

In order to compare the effects of time-varying vortex-induced force coefficients with linear superposition of coefficients at multiple frequencies, the superposition of vortex-induced force coefficients at basic frequency ω_1 and high frequency ω_2 are calculated as follow:

$$CLe_{1+2}(z) = CLe(z,\omega_1) + CLe(z,\omega_2)$$
$$CLa_{1+2}(z) = CLa(z,\omega_1) + CLa(z,\omega_2) \quad (43)$$

And vortex-induced force is reconstructed using equation below:

$$F_{Recon}(z,t) = \frac{\rho D l U^2(z,t)}{2\sqrt{2}\nu_{RMS}(z)} CLe_{1+2}(z)\dot{y}_{multi}(z,t) - \frac{\rho\pi D^2 l}{4} CLa_{1+2}(z)\ddot{y}_{multi}(z,t) \quad (44)$$

Time-space distribution of reconstructed force is shown in Figure 35. Comparing its time-space distribution with that of real force in this case (Figure 25) and comparing time history of reconstructed force with real force at midpoint of riser (Figure 36), it is found that vortex-induced force obtained by direct superposition of vortex-induced coefficients at multiple frequencies cannot reflect the distribution characteristics of real force. It also shows the necessity and superiority of using time-varying vortex-induced force coefficients to reconstruct vortex-induced force.

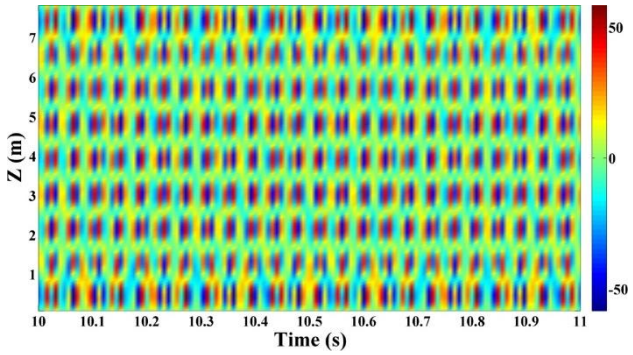

Figure 25 Time-space distribution of vortex-induced force superposition under basic frequency ω_1 and high frequency ω_2

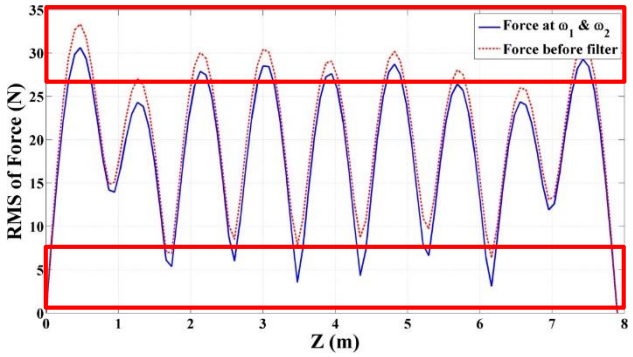

Figure 26 Axial distribution of RMS value of vortex-induced force (blue solid line: superposition of basic frequency ω_1 and high frequency ω_2, red dotted line: before filter)

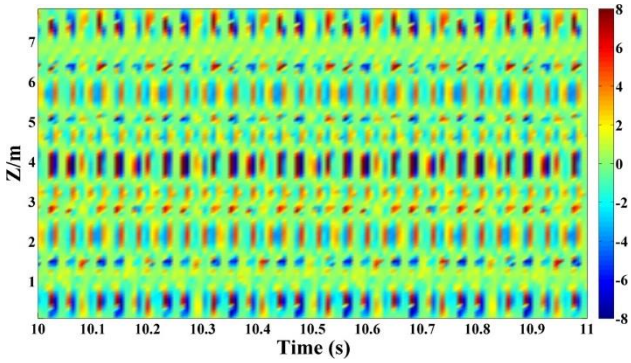

Figure 27 Time-space distribution of excitation coefficient under coupling between basic frequency ω_1 and high frequency ω_2

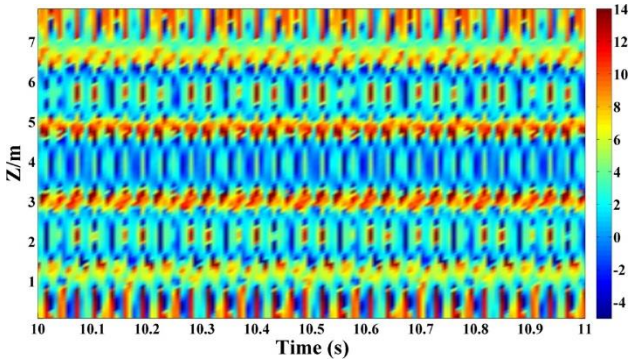

Figure 28 Time-space distribution of added-mass coefficient under coupling between basic frequency ω_1 and high frequency ω_2

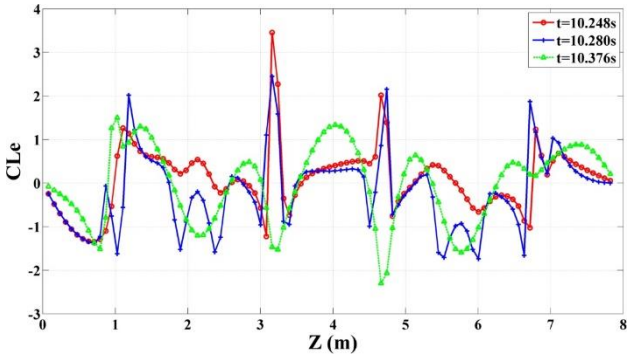

Figure 29 Axial distribution of excitation coefficient at different moment under coupling between basic frequency ω_1 and high frequency ω_2 (red hollow round: t=10.248s, blue plus: t=10.28s, green triangle: t=10.376s)

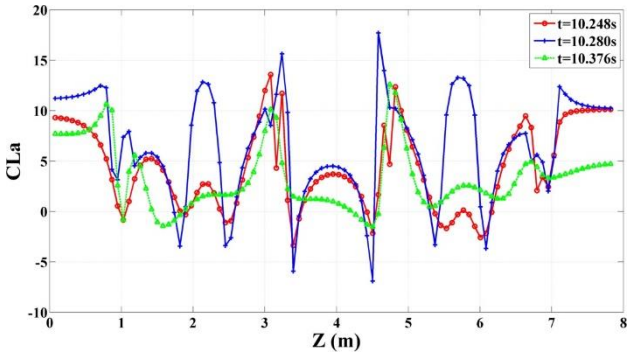

Figure 30 Axial distribution of added-mass coefficient at different moment under coupling between basic frequency ω_1 and high frequency ω_2 (red hollow round: t=10.248s, blue plus: t=10.28s, green triangle: t=10.376s)

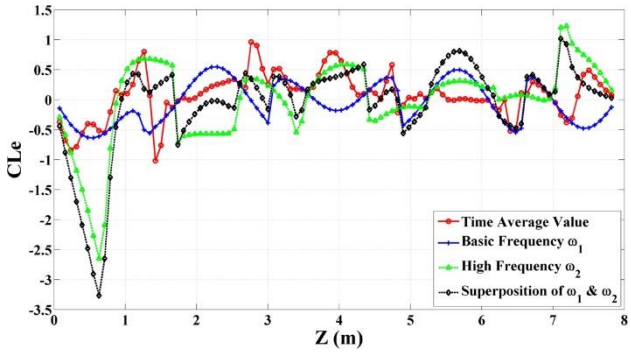

Figure 31 Axial distribution of excitation coefficient (red hollow round: Time-average of time-varying excitation coefficient under coupling between basic frequency ω_1 and high frequency ω_2, blue plus: basic frequency ω_1, black diamond: Superposition of excitation coefficient at basic frequency ω_1 and high frequency ω_2)

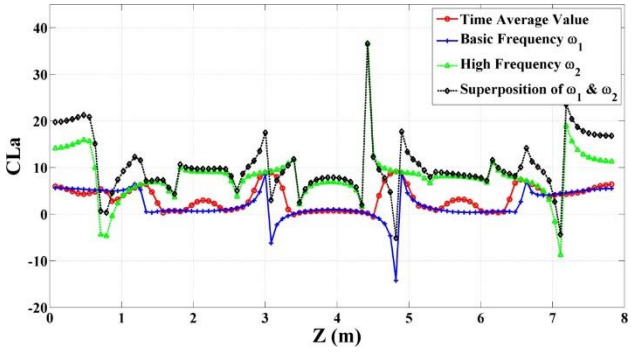

Figure 32 Axial distribution of added-mass coefficient (red hollow round: Time-average of time-varying excitation coefficient considering coupling between basic frequency ω_1 and high frequency ω_2, blue plus: basic frequency ω_1, black diamond: Superposition of excitation coefficient at basic frequency ω_1 and high frequency ω_2)

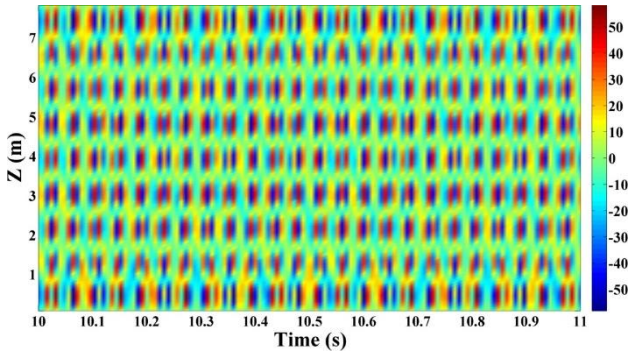

Figure 33 Time-space distribution of force reconstructed from time-varying vortex-induced force coefficients identified from Forgetting Factor Least Square method under coupling of multiple frequency

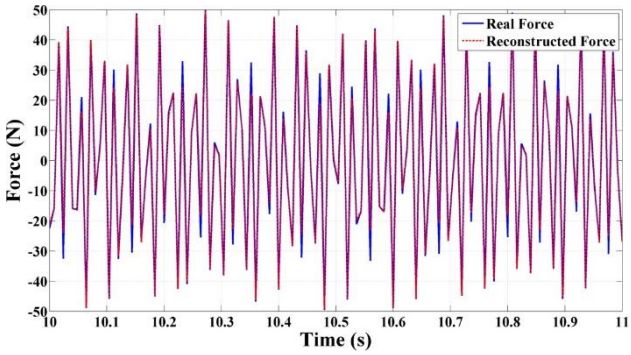

Figure 34 Comparison between real vortex-induced force and force reconstructed from time-varying vortex-induced force coefficients identified by Forgetting Factor Least Square method

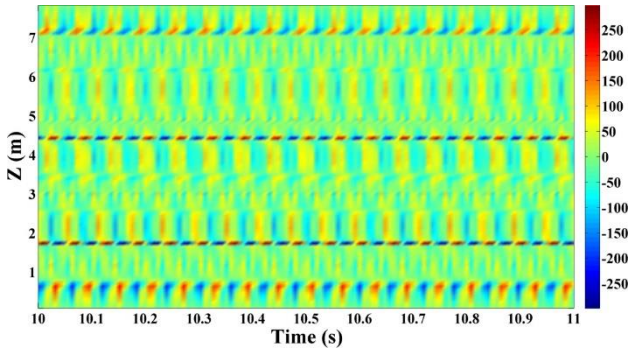

Figure 35 Time-space distribution of vortex-induced force reconstructed from vortex-induced force coefficients superposition of basic frequency ω_1 and high frequency ω_2

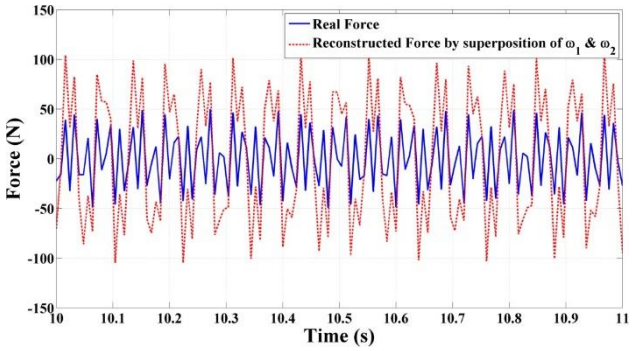

Figure 36 Comparison between real vortex-induced force and force reconstructed from vortex-induced force coefficients superposition of basic frequency ω_1 and high frequency ω_2

CONCLUSION

There are not only the basic frequency component but also the high frequency component in vortex-induced vibration of the real flexible riser. Although the high-frequency component is not obvious in the displacement response, they are equivalent with basic frequency components in the velocity, acceleration and vortex-induced force. At present, the existing method can only identify the vortex-induced force coefficient of single frequency component, but for multi-frequency vortex-induced vibration, the least square method cannot consider the coupling effect between multiple frequencies.

To overcome this shortcoming, this paper introduced a forgetting factor least squares method to identify the time-varying vortex induced force coefficients considering multi-frequency coupling.

First, an ideal model of mass-spring-damping is used to verify that the forgetting factor least squares method can accurately identify the time-varying parameters under multi-frequency coupling. When the system response is single-frequency harmonic, it retrogrades to least squares method and the identification result is consistent with the theoretical solution. When the system response contains multi-frequency components, it shows obvious advantages compared with the least squares method, and the identified system parameters can accurately reconstruct the force signal. Then, this method is used to identify vortex-induced force coefficients of the flexible riser under basic frequency and the results are consistent with the results of the least squares method. This indicates that the least squares method of the forgetting factor proposed in this paper retrogrades to the least squares method when VIV response and the vortex-induced force contain only one single frequency. Finally, the method is used to identify the time-varying vortex-induced force coefficients of the flexible riser under the coupling of basic frequency and high frequency. The identification of time-varying vortex-induced force coefficients are used to reconstruct the vortex-induced force of the flexible riser under the multi-frequency coupling to verify the correctness and applicability of this method.

The results show that vortex-induced force coefficients of the flexible risers change periodically and the time-averaged vortex-induced force coefficients are different from those coefficients at the basic frequency, which results from multi-frequency coupling effect. After superposing vortex-induced force coefficients at basic frequency and that at high frequency, it is quite different from the time-varying coefficient obtained by considering multi-frequency coupling. It is shown that the vortex-induced force coefficients under multiple frequencies cannot be simply superposed in the calculation of vortex-induced force. The forgetting factor least squares method proposed in this paper is an important tool to identify vortex-induced force characteristics under multi-frequency coupling.

ACKNOWLEDGEMENTS

This research was supported by the National Natural Science Foundation of China under Grant Number 51490674

APPENDIX: BENDING STRAIN AND BENDING DISPLACEMENT

The axial tension of the riser model with change periodically when riser undergo vortex-induced vibration. The strain $\varepsilon_{CF1}(z,t)$ and $\varepsilon_{CF2}(z,t)$ measured by FBG strain sensor in the CF direction will include two parts: tensile strain caused by axial tension $\varepsilon_{CF-T}(z,t)$ and bending strain $\varepsilon_{CF}(z,t)$ generated by VIV:

$$\begin{aligned}\varepsilon_{CF1}(z,t)&=\varepsilon_{CF-T}(z,t)+\varepsilon_{CF}(z,t)\\ \varepsilon_{CF2}(z,t)&=\varepsilon_{CF-T}(z,t)-\varepsilon_{CF}(z,t)\end{aligned}\quad(1)$$

Transforming the above equation, then bending strain $\varepsilon_{CF}(z,t)$ in CF direction caused by VIV is:

$$\varepsilon_{CF}(z,t)=\left[\varepsilon_{CF1}(z,t)-\varepsilon_{CF2}(z,t)\right]/2 \quad(2)$$

In IL direction, the average bending deformation of riser is caused by the average drag force. Thereforce, the strain $\varepsilon_{IL1}(z,t)$ and $\varepsilon_{IL2}(z,t)$ measured by FBG strain sensor at the measurement points in the IL direction of riser model consists of three parts: tensile strain caused by aixal tension $\varepsilon_{IL-T}(z,t)$, bending strain generated by VIV $\varepsilon_{IL}(z,t)$ and bending strain $\varepsilon_{mb}(z,t)$ results from average bending:

$$\begin{aligned}\varepsilon_{\mathrm{IL}1}(z,t)&=\varepsilon_{IL-\mathrm{T}}(z,t)+\varepsilon_{IL}(z,t)+\varepsilon_{mb}(z,t)\\ \varepsilon_{\mathrm{IL}2}(z,t)&=\varepsilon_{IL-\mathrm{T}}(z,t)-\varepsilon_{IL}(z,t)-\varepsilon_{\mathrm{mb}}(z,t)\end{aligned}\quad(3)$$

From this equation, bending strain caused by VIV and

average bending at each measurement point $\varepsilon_{IL}(z,t)$:

$$\begin{aligned}\varepsilon_{IL}(z,t) &= \varepsilon_{mb}(z,t) + \varepsilon_{IL}(z,t) \\ &= \left[\varepsilon_{IL1}(z,t) - \varepsilon_{IL2}(z,t)\right]/2\end{aligned} \tag{4}$$

When the bending strain of the riser is obtained, the bending displacement of riser can be obtained by modal analysis. For example, the VIV displacement time history of riser at node z $y(z,t)$ can be expressed as:

$$y(z,t) = \sum_{i=h}^{k} p_i(t)\varphi_i(z), \quad z \in [0,L] \tag{5}$$

Where $\varphi_i(z)$ is is the ith displacement mode of the riser in the local coordinate system, and $p_i(t)$ is time history of displacement weight.

For bending displacement $y(z,t)$ and bending strain $\varepsilon(z,t)$ satisfy the equation below:

$$\frac{\partial^2 y(z,t)}{\partial z^2} = -\frac{\varepsilon(z,t)}{R} \tag{6}$$

From equation (5) and (6), the bending strain $\varepsilon(z,t)$ can be obtained:

$$\varepsilon(z,t) = -R\sum_{i=h}^{k} p_i(t)\varphi_i''(z) \tag{7}$$

Therefore, when the bending strain $\varepsilon_{CF}(z,t)$ of the riser in CF direction is obtained from equation (2), time history of displacement mode weight $p_i(t)$ can be obtained according to equation (7). Then the bending displacement response $y(z,t)$ of the riser in CF direction can be obtained by equation (5). Similarly, bending displacement $x(z,t)$ of riser in IL direction can be obtained from bending strain $\varepsilon_{IL}(z,t)$ by equation (4)

REFERENCES

[1]. Gopalkrishnan, R., Vortex-induced forces on oscillating bluff cylinders. Massachusetts Institute of Technology, 1993.

[2]. Larsen, C.M., R. Yttervik and K. Aronsen. Calculation of In-Line Vortex Induced Vibrations of Free Spanning Pipelines. in ASME 2007 International Conference on Offshore Mechanics and Arctic Engineering. 2007.

[3]. Jauvtis, N. and C. Williamson, The effect of two degrees of freedom on vortex-induced vibration at low mass and damping. Journal of Fluid Mechanics, 2004. 509: p. 23-62.

[4]. Dahl, J. and J. Dahl, Vortex-induced vibration of a circular cylinder with combined in-line and cross-flow motion. Massachusetts Institute of Technology, 2008.

[5]. Marcollo, H. and J.B. Hinwood, On shear flow single mode lock-in with both cross-flow and in-line lock-in mechanisms. Journal of Fluids and structures, 2006. 22(2): p. 197-211.

[6]. Sumer, B.M. and J. Fredsøe, Hydrodynamics Around Cylindrical Structures. Coastal Engineering, 2006. 33(33): p. 69-69.

[7]. Vandiver, J.K., V. Jaiswal and V. Jhingran, Insights on vortex-induced, traveling waves on long risers. Journal of Fluids and Structures, 2009. 25(4): p. 641-653.

[8]. Vandiver, J.K., et al. Fatigue damage from high mode number vortex-induced vibration. in 25th International Conference on Offshore Mechanics and Arctic Engineering. 2006: American Society of Mechanical Engineers.

[9]. Wu, J., et al., Vortex-induced vibration of a flexible cylinder: Interaction of the in-line and cross-flow responses. Journal of Fluids & Structures, 2016. 63: p. 238-258.

[10]. Song, L., et al., An investigation into the hydrodynamics of a flexible riser undergoing vortex-induced vibration. Journal of Fluids and Structures, 2016. 63: p. 325-350.

[11]. Fang, S.M., et al., VIV response of a flexible cylinder with varied coverage by buoyancy elements and helical strakes. Marine Structures, 2014. 39: p. 70-89.

[12]. Li, L., et al., Dynamic responses of floating fish cage in waves and current. Ocean Engineering, 2013. 72: p. 297-303.

[13]. Lie, H., K. Mo and J.K. Vandiver. VIV model test of a bare-and a staggered buoyancy riser in a rotating rig. in Offshore Technology Conference. 1998: Offshore Technology Conference.

[14]. Li, L., et al. Experimental investigation on vortex-induced vibration of risers with staggered buoyancy. in ASME 2011 30th International Conference on Ocean, Offshore and Arctic Engineering. 2011: American Society of Mechanical Engineers.

[15]. Gopalkrishnan, R., Vortex-induced forces on oscillating bluff cylinders. 1993, DTIC Document.

[16]. Ding, F. and T. Chen, Performance bounds of forgetting factor least-squares algorithms for time-varying systems with finite measurement data. IEEE Transactions on Circuits and Systems I: Regular Papers, 2005. 52(3): p. 555-566.

[17]. Paleologu, C., J. Benesty and S. Ciochina, A robust variable forgetting factor recursive least-squares algorithm for system identification. IEEE Signal Processing Letters, 2008. 15: p. 597-600.

[18]. Chavent, G. Identification of distributed parameter systems: about the output least square method, its implementation and identifiability. in Proc. 5th IFAC Symposium on Identification and System Parameter Estimation. 1979.

[19]. Lie, H. and K.E. Kaasen, Modal analysis of measurements from a large-scale VIV model test of a riser in linearly sheared flow. Journal of Fluids & Structures, 2006. 22(22): p. 557-575.